Reconfigurable RF Transmitters for C-Band and X-Band:

Design, Development and Testing

by

Samuel Gordon

A Thesis Presented in Partial Fulfillment
of the Requirements for the Degree
Master of Science

Approved April 2022 by the
Graduate Supervisory Committee:

Daniel Bliss, Co-Chair
Philip Mauskopf, Co-Chair
Antonia Papandreou-Suppappola

ARIZONA STATE UNIVERSITY

May 2022

ABSTRACT

This thesis covers the design, development and testing of two high-power radio frequency transmitters that operate in C-band and X-band (System-C/X). The operational bands of System-C/X are 3–6 GHz and 8–11 GHz, respectively. Each system is designed to produce a peak effective isotropic radiated power of at least 50 dBW. The transmitters use parabolic dish antennas with dual-linear polarization feeds that can be steered over a wide range of azimuths and elevations with a precision of a fraction of a degree.

System-C/X's transmit waveforms are generated using software-defined radios. The software-defined radio software is lightweight and reconfigurable. New waveforms can be loaded into the system during operation and saved to an onboard database. The waveform agility of the two systems lends them to potential uses in a wide range of broadcasting applications, including radar and communications.

The effective isotropic radiated power and beam patterns for System-C/X were measured during two field test events in July 2021 and January 2022. The performance of both systems was found to be within acceptable limits of their design specifications.

ACKNOWLEDGMENTS

Many talented people had a hand in the design, development and testing of the two RF systems which are the subject of this thesis, and I owe a debt of gratitude to each of them. The thesis itself is the culmination of a journey that started in Tempe, Arizona, in 2016 and ended in Woburn, Massachusetts, in 2022. During those six years there were times when I was on the verge of throwing in the towel. This document is a testament to the combined support and encouragement of those who urged me to stay the course.

This material is based on work supported by AFRL under Contract No. FA488720P0100. Any opinions, findings, or conclusions expressed in this material are those of its authors and do not necessarily reflect the views of AFRL.

TABLE OF CONTENTS

CHAPTER Page

LIST OF TABLES

LIST OF FIGURES

Chapter 1

INTRODUCTION

This thesis covers the design, development and testing of two high-power radio frequency (RF) transmitters that operate in C-band and X-band (System-C/X). The operational bands of System-C and System-X are 3–6 GHz[1] and 8–11 GHz, respectively. Each system is designed to produce a peak effective isotropic radiated power (EIRP) of at least 50 dBW.

The two systems' transmit waveforms are generated using software-defined radios (SDRs) (see, e.g., Wyglinski et al. (2018)). The SDR software is lightweight and reconfigurable. The transmitters use dual-linear polarization parabolic dish antennas to direct their signal power into narrow beams with half-power beam widths (HPBWs) of 3–6 degrees. The beams can be steered over a wide range of azimuths and elevations with a precision of a fraction of a degree. The waveform agility of the two systems lends them to potential uses in a wide range of broadcasting applications, including radar and communications.

While similar systems might exist (see, e.g., Skolnik (1980)), System-C/X have been designed to be as flexible as possible from a waveform generation standpoint. New waveforms can be quickly programmed into the system during operation and saved to an onboard database for future use.

[1]This is a compromise between the IEEE definitions of S-band and C-band: IEEE radar band definitions

The thesis is organized as follows:

- Chapter 2 describes the design process for System-C/X.
- Chapter 3 discusses specific aspects of the high-power amplifier (HPA) development process.
- Chapter 4 describes the field testing that was done to characterize the performance and functionality of each system, as well as the data analysis that was done to verify that the systems meet their key performance requirements.
- Chapter 5 discusses lessons learned from the work described in the previous chapters, as well as potential improvements that can be made to future versions of the systems.

Chapter 2

DESIGN

The design phase of the two systems starts with a general concept-of-operations (CONOPS) and a spending budget for a first-run prototype. Although cost is an important factor in the design and selection of specific components and subsystems, it will not be considered in this document.

The CONOPS is used to derive a set of system requirements and to sketch out a high-level system architecture. Then, using the hardware budget as a guide, the system architecture is populated with specific components and subsystems whose capabilities satisfy each of the system requirements to the greatest extent possible. In some cases, the chosen components add new features to the system that aren't formally required. Once all of the components have been selected and formed into subsystems, the system can be described by its specifications.

Before certain system specifications can be assembled into a datasheet, they must be verified through testing and characterization. The performance testing for System-C/X is discussed in Chapter 4.

2.1 CONOPS to System Requirements

The general CONOPS for System-C/X is to broadcast user-defined arbitrary waveforms in a specified direction with EIRPs of at least 50 dBW. The dish antennas should be able to be steered at drive rates of several degrees-per-second in both azimuth and elevation. When considering components, commercial off-the-

shelf (COTS) or semi-custom COTS components should be chosen over custom components wherever possible. The instantaneous field of view (IFOV) for the two systems should be a few square-degrees. From an architecture standpoint, the systems are meant to be portable using a conventional flatbed truck, and able to be assembled and broken down by one or two individuals using few to no specialized tools. Therefore, if the systems are to be modular, each individual module should weigh $\lesssim 50$ lb.

System-C/X should be operable in a desert environment. Both systems will need to operate continuously for up to 12 hours in this environment before any generators need to be refueled. Each subsystem must be rugged enough to tolerate the year-round conditions that are typical of deserts. For the purposes of this document, the desert environment is defined as ambient temperatures ranging from 0–50 °C (not accounting for additional heating due to solar radiation), occasional light rain, and occasional heavy rain with high-winds that carry large amounts of dust. The systems will be operated in remote locations, and will therefore need to support remote operations.

A core set of system requirements can be derived from the CONOPS described above. These requirements are listed in Table 1. Unless specified in the table, the requirements apply to both System-C/X. Requirements included in the threshold column are a higher priority to meet than their corresponding objective requirements.

Requirement	Threshold	Objective
Operational band	3–6 GHz (C) 8–11 GHz (X)	
EIRP	$\gtrsim 50$ dBW	
Modulation	Unmodulated, LFM, phase-coded	
IBW	≥ 20 MHz	
Duty cycle	20%	100%
Polarization	Dual-linear polarization	
Pointing control	Independent azimuth and elevation	
Drive rate (az. and el.)	$\sim$10 deg/s	
Pointing accuracy	1 deg	< 1 deg
IFOV	A few square degrees	
Power consumption	$\lesssim 2$ kW	Minimize
Remote operation	LAN	Wireless
Size and Weight	Each module $\lesssim 50$ lb	
GPS	Include GPS antenna	
Control interface	Cross-platform GUI	
Thermal	Operable from 0–50 °C	
Environmental	Dust, moisture, light rain, moderate wind	

Table 1: High-level system requirements for System-C/X, with their associated threshold and objective values (if applicable).

2.2 System Requirements to a System Architecture

The system architecture for System-C/X is developed using the system requirements listed in Table 1. Key aspects of the architecture are considered individually below:

RF power: The EIRP requirement of $\gtrsim 50$ dBW for both systems indicates the need for a HPA and high gain antenna. The antenna should support dual-linear polarizations. A parabolic dish antenna is chosen as the most suitable architecture to meet these needs (see, e.g., Balanis (2015)). Regarding the HPA, it would be possible to design the system around either a solid-state power amplifier (SSPA) or a traveling-wave tube amplifier (TWTA) (see Section 2.3.1).

Waveform generation: To satisfy the waveform modulation requirements of linear-frequency modulation (LFM) and phase-coding, the HPA should be driven by a waveform generation system that can be easily reconfigured. SDRs are chosen for this purpose due to their high flexibility and low cost and complexity relative to other systems (e.g., field-programmable gate arrays (FPGAs)). RF front ends (RFFEs) will be added to the SDRs to provide filtering and signal conditioning for interfacing with the HPAs. For System-X, an RF upconverter will be required to translate the intermediate frequency (IF) output of the SDR to X-band.

Command and control: Since the systems will need to be remotely operable, the command and control (C2) system will be based on a server-client architecture in which a single server can control multiple systems on the same network. System-C/X will each have their own computer that accepts commands from the central server and exercises control over its various subsystems.

Power consumption: Electrical power will be supplied to the system using gas-powered generators. To support continuous operation in a desert environment, critical subsystems will need to be actively cooled, moisture resistant and rugged.

Size, weight and power (SWaP): Given the weight requirement of $\lesssim 50$ lb for each subsystem, heavier subsystems should be designed so that they can be broken down into smaller modules that can be managed by one or two individuals. Additionally, it should be possible to assemble and disassemble the subsystems using standard hand tools.

Given the above considerations, the key subsystems for System-C/X are:

- Dishes and antenna feeds
- Positioner units and antenna mounts
- Electronics (SDRs, RFFEs, client computers)

- Control software and user interface

A high-level diagram of the general system architecture is shown in Figure 1.

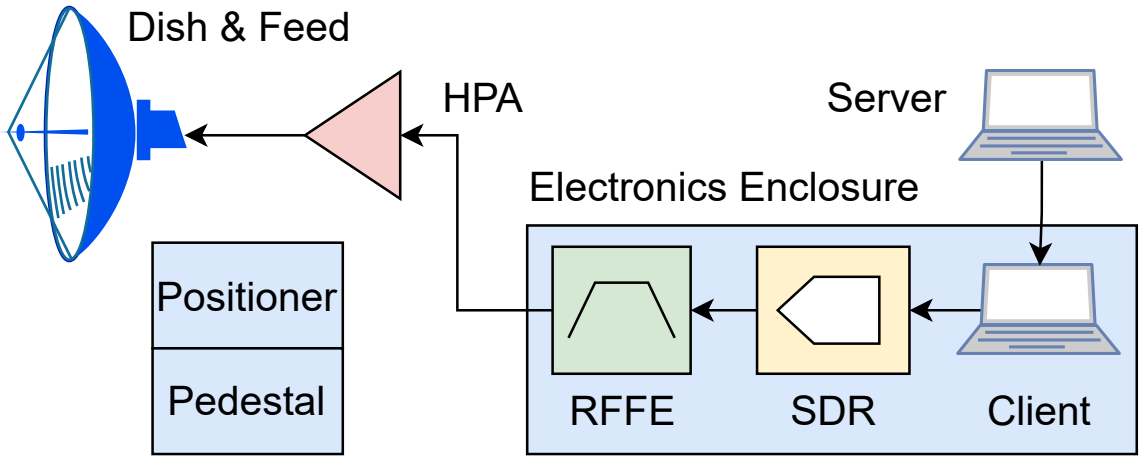

Figure 1: General system architecture diagram for System-C/X.

In the following sections, the generic system architecture shown in Figure 1 will be refined to match the requirements that are unique to System-C/X.

2.3 System Specifications

The following sections describe the subsystem specifications for the subsystems listed in Section 2.2.

2.3.1 HPAs

SSPAs and TWTAs are complementary technologies with relative strengths and weaknesses (see, e.g., Montgomery and Courtney (2017)). While SSPAs are still an evolving technology, TWTAs have long been used for microwave amplification in close to their current form (Pierce and Field (1947)). Although TWTAs generally

provide higher output powers over broader operational bands than SSPAs (Pozar (2011)), their operational lifespans are limited by the fragility of the traveling-wave tube (TWT). Both SSPAs and TWTAs require heatsinking to conduct heat away from either the output transistors or the TWT, which adds to their size and weight. Since solid-state devices are typically much smaller in size than TWTs, the heat that's generated by SSPAs is concentrated in a much smaller area. This makes thermal regulation more challenging in comparison to TWTAs.

Considering the points listed above, TWTAs were selected for System-C/X. The TWTA for each system is a semi-custom COTS solution provided by Quarterwave Corp[2]. To meet the size and weight requirements for the two systems, a modular architecture was adopted for the TWTAs in which each system consists of three modules: An RF powerhead that houses the TWT and other RF components, a power supply unit (PSU) that supplies electrical power as a well as a data link to the RF powerhead, and a liquid chiller unit.

The RF powerhead is designed to sit on-axis with the antenna dish, while the PSU and chiller rest on the ground. Power, communication and cooling for the RF powerhead are provided by cables and hoses that run between the three modules. These cables must be managed appropriately while the antennas are being pointed and scanned.

In the following, the amplifiers for System-C/X will be referred to as HPA-C and HPA-X. The specifications for HPA-C/X are listed in Table 2.

The following sections describe the sub-modules of HPA-C/X.

[2]Quarterwave Corp

Specification	HPA-C	HPA-X
Vendor	Quarterwave Corp.	
Operational band	3–6 GHz	8–11 GHz
Saturated output power	56 dBm	49 dBm
Duty cycle (max.)	40%	
Operational mode	Gated	CW
Output VSWR	2:1	
Size	Single-person lift	
Weight (RF powerhead)	33 lb	20 lb
On/off-axis	RF powerhead on-axis	
Power consumption	∼2 kW	∼1.5 kW
Cooling system	Liquid chiller	
Coolant type	PG based coolant (non-toxic)	
Thermal	≤ 50 °C	
Environmental	Dust and moisture resistant	

Table 2: HPA-C/X specifications.

2.3.1.1 HPA RF Powerheads

A photo of HPA-X's RF powerhead is shown in Figure 2. Although HPA-C's powerhead is slightly larger than HPA-X's, their general appearance and interfaces are the same. The RF powerheads contain the TWT, a solid-state RF preamplifier and a microcontroller unit (MCU). The RF powerheads have the following interfaces:

- High and low voltage ports
- Type-N connectors for the input and output RF signals
- Input and output valves for coolant

The RF powerheads are designed to attach to the antenna feed assembly using a mounting plate, and sit on-axis during system operation.

Figure 2: HPA-X RF powerhead.

2.3.1.2 HPA Power Supplies

Figure 3a and Figure 3b are photos of the HPA-C/X PSUs. HPA-C's PSU is larger than HPA-X's, and has a touchscreen user interface (UI). Both PSUs can be controlled either locally by using the buttons on the front panel, or remotely via an Ethernet interface. The state of the HPAs is indicated on their front panels in either the UI (for HPA-C) or with status LEDs. The PSUs contain MCUs that interact with the MCU in the powerheads to govern the behavior of the TWT and monitor the system health by reading out temperature and voltage sensors in both the PSUs and powerheads. High and low voltages (both power and signal) are routed to the powerhead using cable assemblies. The design of HPA-X's PSU requires that it be cooled using a chiller unit.

As noted in Table 2, HPA-C/X are operated using different modes. HPA-X is operated in continuous wave (CW) mode, which means that the TWT grid is always active during normal operation, even when the RF signal is pulsed. In CW mode, the TWT dissipates more power, and there is a slightly higher noise floor at the RF-output port during RF pulse dwell times than if the TWT were to be turned off during the dwells.

Because HPA-C dissipates more power than HPA-X, the system is operated in

gated mode. In gated mode, an external trigger is used to gate the TWT grid during dwell times. The pulse repetition interval (PRI) of the trigger, or gating signal, must be synchronized to the PRI of the RF signal. For System-C, this gating signal is generated using the second channel of the N300 SDR (see Section 3.3). The gating signal is input to the PSU via an SMA port.

(a)

(b)

Figure 3: (a) HPA-C PSU (b) HPA-X PSU.

2.3.1.3 HPA Chillers

A chiller unit is shown in Figure 4. System-C/X each have their own chiller, and the two units are identical. The coolant is propylene glycol (PG)-based and non-toxic.

Figure 4: An HPA chiller unit.

2.3.2 Software-Defined Radios

The SDRs chosen for System-C/X are Ettus Research[3] USRPs (Universal Software Radio Peripherals). Although System-C/X share a common waveform generation requirement, a different USRP was chosen for each system. Because HPA-X is operated in CW mode, System-X requires a single transmit (TX) channel. Therefore, an Ettus B205mini-i was selected due to its relatively low size, weight, power and cost (SWaP-C).

[3]Ettus Research's website.

Because System-C requires two TX channels, one for the RF output and one for the gating signal, a dual-channel SDR was required. An Ettus N300 SDR was selected for two primary reasons. First, it supports a higher IBW (instantaneous bandwidth) than the B-series of Ettus USRPs (100 MHz vs 56 MHz for a single channel). While the N300's maximum IBW exceeds the threshold requirement of at least 20 MHz, it provides the option to implement additional waveform types in the future. Second, the N300 contains an embedded CPU (central processing unit), meaning that unlike System-X, System-C doesn't require a dedicated control computer inside its electronics enclosure. Specifications for the two SDRs are listed in Table 3.

Specification	N300	B205mini-i
Vendor	Ettus Research	
Part	N300	B205mini-i
Operational band (IF)	70 MHz–6 GHz	10 MHz–6 GHz
IBW	~80 MHz	~45 MHz
Number TX channels	2	1
FPGA	Kintex-7 RFNoC	Xilinx Spartan-6
CPU	Dual-core ARM Cortex-A9	Minisforum HM50
DAC resolution	14-bit	12-bit
Thermal	0–50 °C	-40–70 °C
Power consumption	50–80 W	USB 3.0 bus power

Table 3: SDR specifications for System-C/X.

2.3.3 Antennas

The two antenna systems (antenna-C/X) were developed by mWAVE Industries[4]. Antenna-C/X are semi-custom COTS parabolic dish antennas that support dual-linear polarizations. The antennas share several specifications, but differ in their operational bands, beamwidths, gain and power handling. The key specifications for antenna-C/X are listed in Table 4.

Both dishes are 0.9 m in diameter, and include a radome. The dishes have HPBWs of ∼3 degrees and ∼6 degrees, respectively. Antenna-X's feed coupling uses rectangular waveguide, and antenna-C's uses coaxial cables. Both feeds include a polarization switch that can be electronically controlled during system operation using switch controller units. These units are connected to the antenna feed assembly with cables that are ∼6 ft in length.

The feed assemblies for antenna-C/X are custom-made by mWAVE and are similar in design. They sit behind the dishes and support the polarization switches, waveguide plumbing and RF powerheads.

The positioner units (positioner-C/X) are COTS units sourced from Nextmove Technologies[5]. While positioner-C/X are identical, System-C uses a quadpod pedestal while System-X uses a tripod pedestal. Because System-C has more weight on-axis due to HPA-C's larger RF powerhead, the quadpod was chosen over the tripod for additional stability. Power for the positioner unit is provided using power-over-Ethernet (PoE). Specifications for positioner-C/X are listed in Table 5.

[4]mWAVE LLC's website.

[5]Nextmove Technologies' website.

Specification	System-C	System-X
Vendor	mWAVE Industries LLC	
Operational band	3–6 GHz	8–12 GHz
Dish diameter	0.9 m	
Dish type	Axisymmetric aluminum reflector	
Feed	Prime focus, dual-linear polarization	
Polarization switching	Solid-state	Solenoid relay
Feed coupling	Coax	Waveguide
Gain (mid-band)	28 dBi	36 dBi
HPBW (mid-band)	∼5 deg	∼2.5 deg
IFOV	6 x 6 deg	3 x 3 deg
Power handling (Peak/Average)	500 W/150 W	400 W/150 W
Max. input return loss	7.8 dB	15 dB
Operational wind speed	20 mph (62 mph survivable)	
Weight	36 lb (with radome)	
On-axis cross-pol	< 30 dB	
Thermal	≤ 50 °C	

Table 4: Antenna-C/X specifications.

Specification	Positioner-C & Positioner-X
Vendor	Nextmove Technologies
Azimuth range	± 270 deg
Elevation range	± 95 deg
Azimuth drive rate	12 deg/s
Elevation drive rate	5 deg/s
GPS	GPS antenna included
Compass	Magnetic compass in mount
Weight	Positioner: 40.5 lb, Pedestal: 25 lb
Operational wind speed	20 mph (62 mph survivable)
Power consumption	16–95 W
Thermal	-30–60 °C

Table 5: Positioner-C/X specifications.

Figure 5a and Figure 5b show the System-C/X antenna and positioner assemblies

(a)

(b)

Figure 5: System-C antenna and pedestal assembly (b) System-X antenna and pedestal assembly.

in their fully assembled state. The HPA powerheads are mounted on the back of the feed assemblies.

2.3.4 RF Front Ends

RFFEs were added to the System-C/X SDRs to provide signal conditioning for the IF output of the SDRs. For System-X, the RFFE also provides frequency translation to X-band. DC blocks were added to the TX ports of each SDR to eliminate any DC offset.

2.3.4.1 C-band RF Front End

The purpose of the C-band RFFE is to filter out any undesired frequency content above the maximum IF output frequency of 6 GHz. Figure 6 shows a diagram of the IF signal chain. The RFFE consists of a low-pass filter (LPF) and high-pass filter (LPF) that together form a band-pass filter (BPF) with 3 dB points of ∼2.275 GHz and ∼6 GHz. The insertion loss of the BPF is minimal.

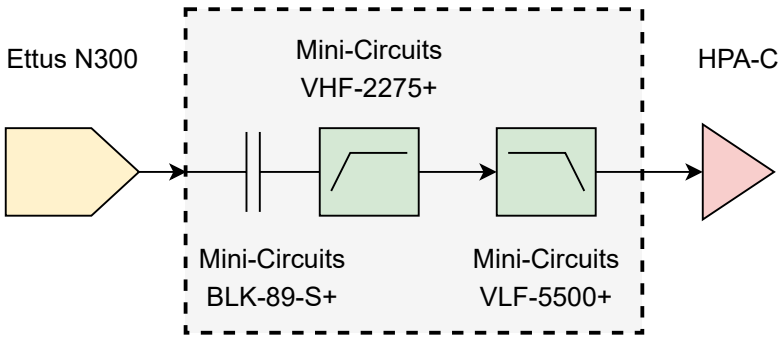

Figure 6: A diagram of the C-band RFFE electronics.

2.3.4.2 X-band RF Front End

The X-band RFFE consists of a DC block, IF BPF and an upconversion stage that's responsible for converting the IF frequencies to an RF band that spans 8–11 GHz. The IF BPF is more than 100 MHz wide, and does not limit the IBW of the system. A diagram of the upconverter electronics is shown in Figure 7a, and a photo of the electronics is shown in Figure 7b.

Although the B205mini-i has a usable IF band of 70 MHz–6 GHz, all System-X waveforms are centered at an IF frequency of 3.5 GHz. This center frequency was selected because it results in no significant in-band spurs in the RF band (the 3rd harmonic of the IF center frequency, 10.5 GHz, is greatly attenuated by the mixer). Figure 8a shows the RF frequencies and relative power levels (dBc relative to the IF carrier level) of mixer spurs in the RF band.

To achieve the upconversion, a double-balanced mixer is used with high-side local-oscillator (LO) injection (the LO frequency is higher than the RF frequencies). The LO is a tunable synthesizer (Windfreak SynthHD[6]) that has a tuning increment of ~100 Hz. Frequency tuning in the RF band is achieved by changing the LO frequency while the IF center frequency remains fixed.

Following the mixer stage, the lower sideband (LSB) of the RF signal is selected using a COTS BPF that covers 8–11 GHz. This first filter serves to attenuate the out-of-band mixer products before the signal enters a single amplification stage. The amplifier is followed by a custom BPF from Anatech Electronics[7]. The custom BPF

[6]Windfreak Technologies, LLC website.

[7]Anatech Electronics website.

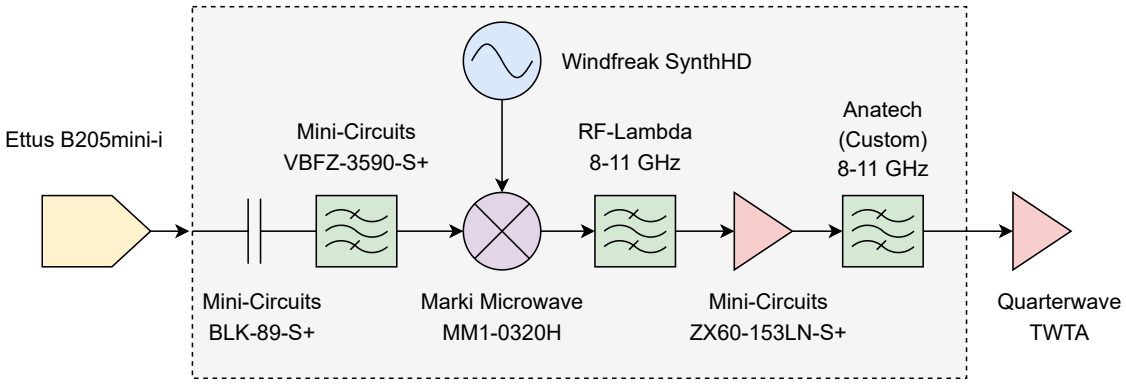

(a)

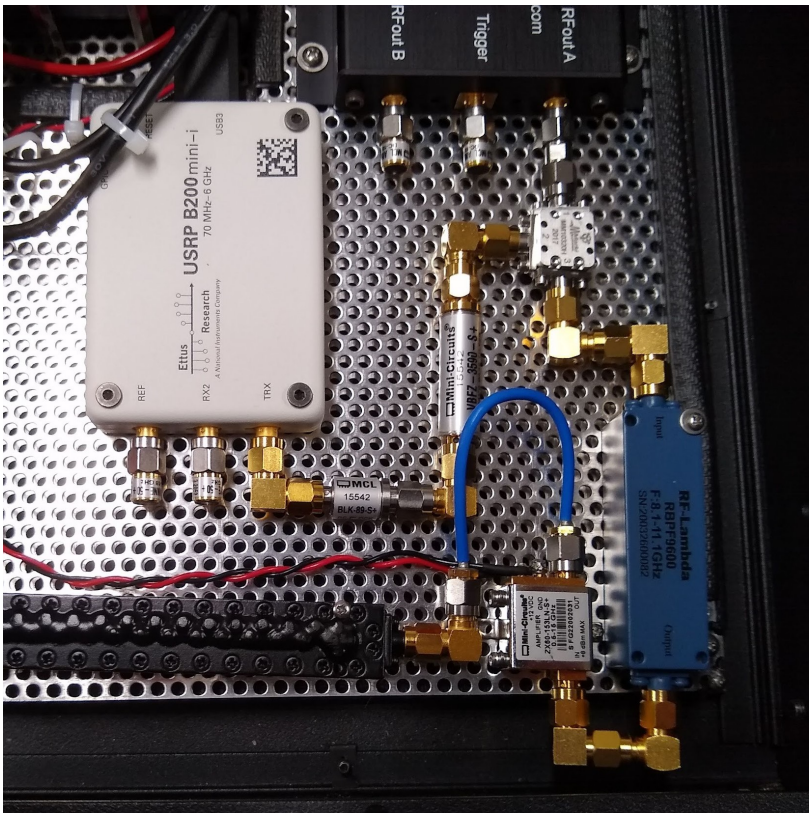

(b)

Figure 7: (a) A diagram of the X-band upconverter signal chain (b) A photo of the X-band upconverter electronics.

is a cavity filter (see, e.g., Hunter (2001)) with a very narrow transition band (insertion loss of > 60 dB at 7.5 GHz and 11.5 GHz) that serves to eliminate any out-of-band frequency components that are produced by the mixer, amplifier and LO. Figure 8b shows a comparison between the simulated and measured S_{21} of the custom BPF (see, e.g., Pozar (2011) for a detailed overview of scattering parameters).

Specification	Value
Operational band	8–11 GHz
Local oscillator	Windfreak SynthHD
IF center frequency	3.5 GHz
IBW	≤ 100 MHz
Frequency tuning resolution	$\sim$100 Hz
Power consumption	5.5 W
Thermal	≤ 50 °C

Table 6: X-band upconverter specifications.

2.3.5 Electronics Enclosures

Custom electronics enclosures were developed for System-C/X to house the SDRs, RFFEs, control computers, positioner unit PoE supplies and Ethernet switch. Three views of System-X's enclosure are shown in Figure 9.

Each system's electronics enclosure consists of a 4U (standard rack units) transport case containing an inner 2U rackmount chassis that houses the electronics. The exterior of the case is coated with a tan sealant that provides increased resistance to wear and tear and reduces the thermal load on the electronics from solar radiation.

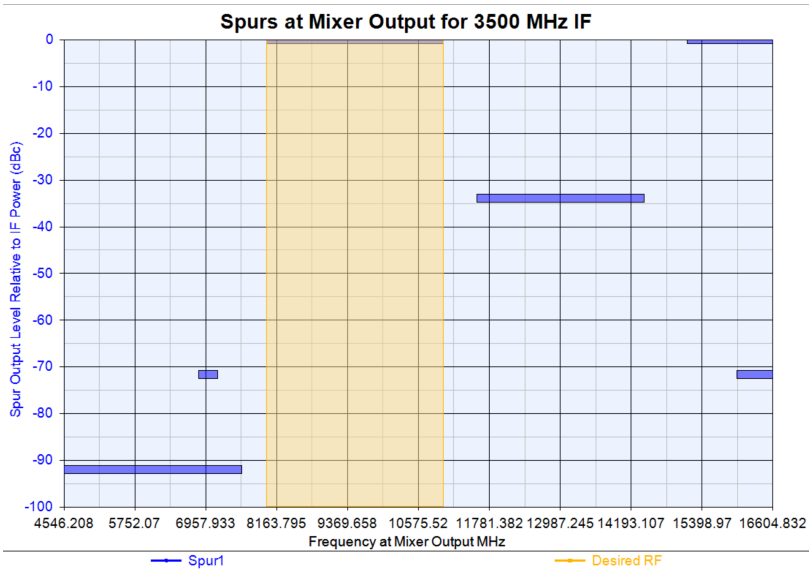

(a)

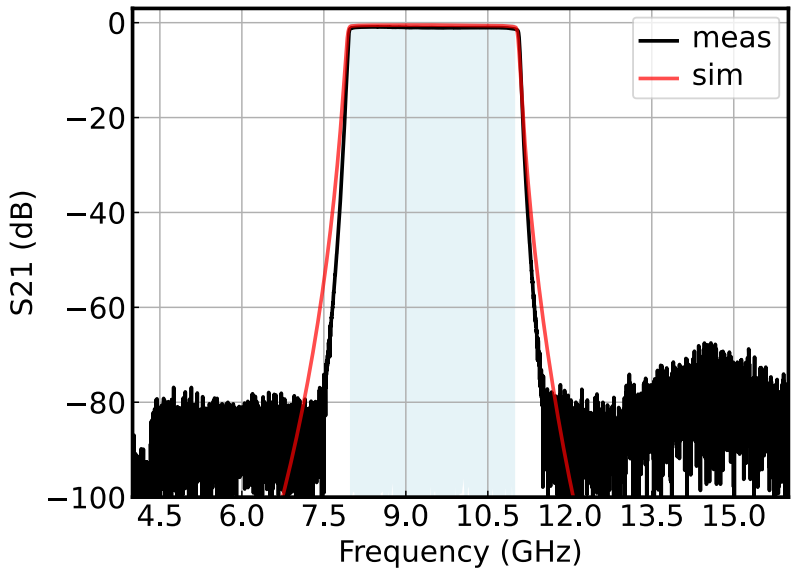

(b)

Figure 8: (a) A chart showing the locations of frequency spurs in X-band (b) The passband of the custom X-band BPF.

(a)

(b)

(c)

Figure 9: Three views of an electronics enclosure: (a) front (b) top (c) front panel removed.

Overhead views of the contents of System-C/X's 2U electronics chassis are shown in Figure 10 and Figure 11. All of the signals that are generated inside of the chassis are routed through bulkhead connectors on its front panel to bulkhead connectors on the front panel of the transport case. The front panel interfaces are:

- Type-N connector (RF-out)
- SMA connector (only for System-C, for the TWT gating signal)
- PoE (for the positioner unit)
- Ethernet for the HPA
- Ethernet for communicating with the server

AC electrical power is routed through the back panel of the outer box via a waterproof, locking socket. The internal electronics are actively cooled by a thermostat-controlled thermoelectric cooler that's mounted in the top face of the transport case.

2.3.6 Software and User Interface

System-C/X are controlled through a graphical user interface (GUI) that's accessible via an internet browser. The GUI runs on a server computer that communicates with the client computers in System-C/X over an Ethernet switch. Client software on the System-C/X computers receives commands through the GUI and executes them. The client software also reports system health and status information to the server, which displays it in the GUI and logs it for future analysis. The software allows for real-time monitoring and control over the various subsystems. The GUI, server and client software have been developed by Arizona State University (ASU).

The server, client and GUI software are all written in Python, which makes it

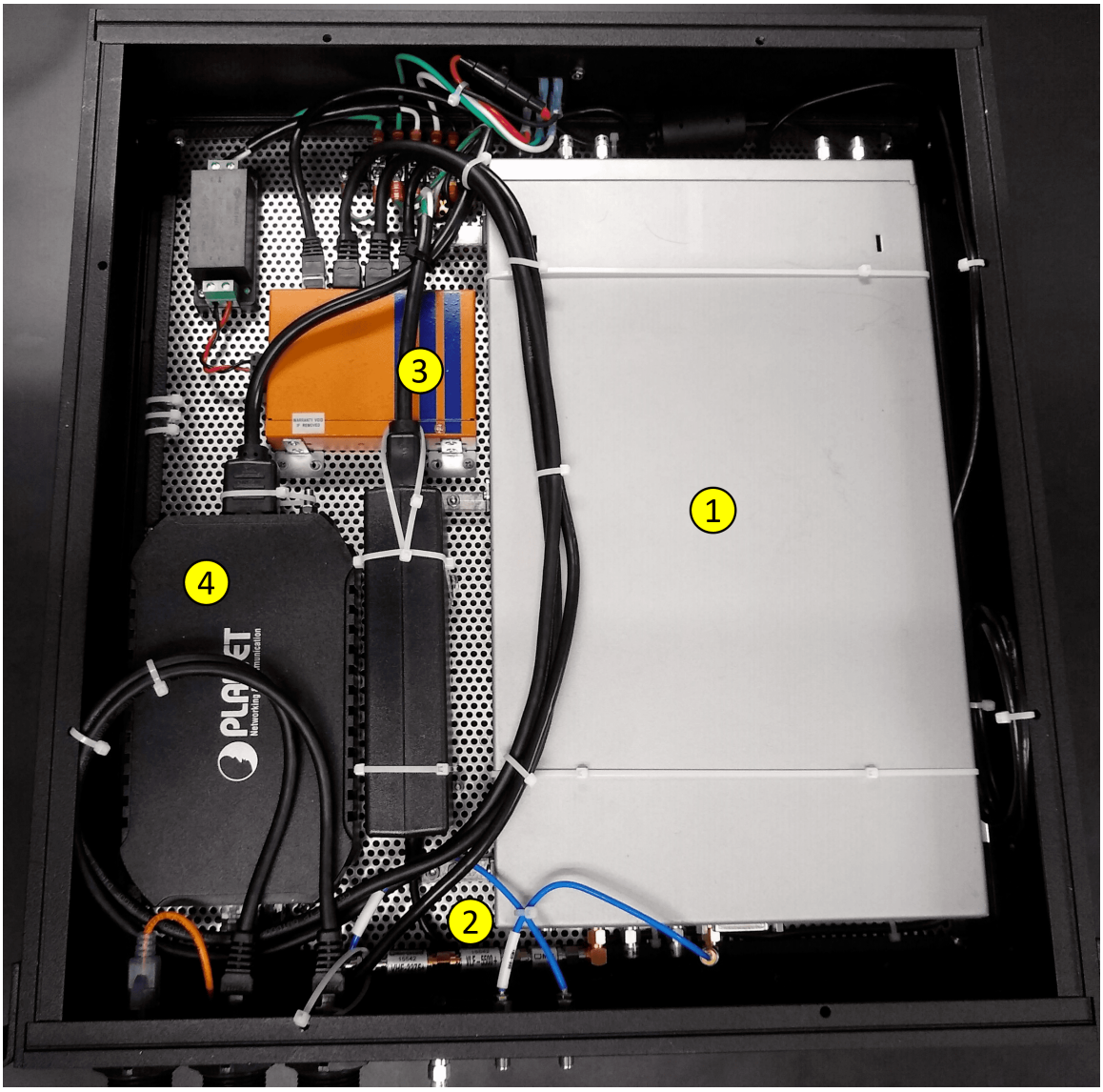

Figure 10: A photo of the components inside System-C's electronics enclosure. Key components are numbered: (1) Ettus N300 SDR (2) RFFE (3) Ethernet switch (4) PoE supply.

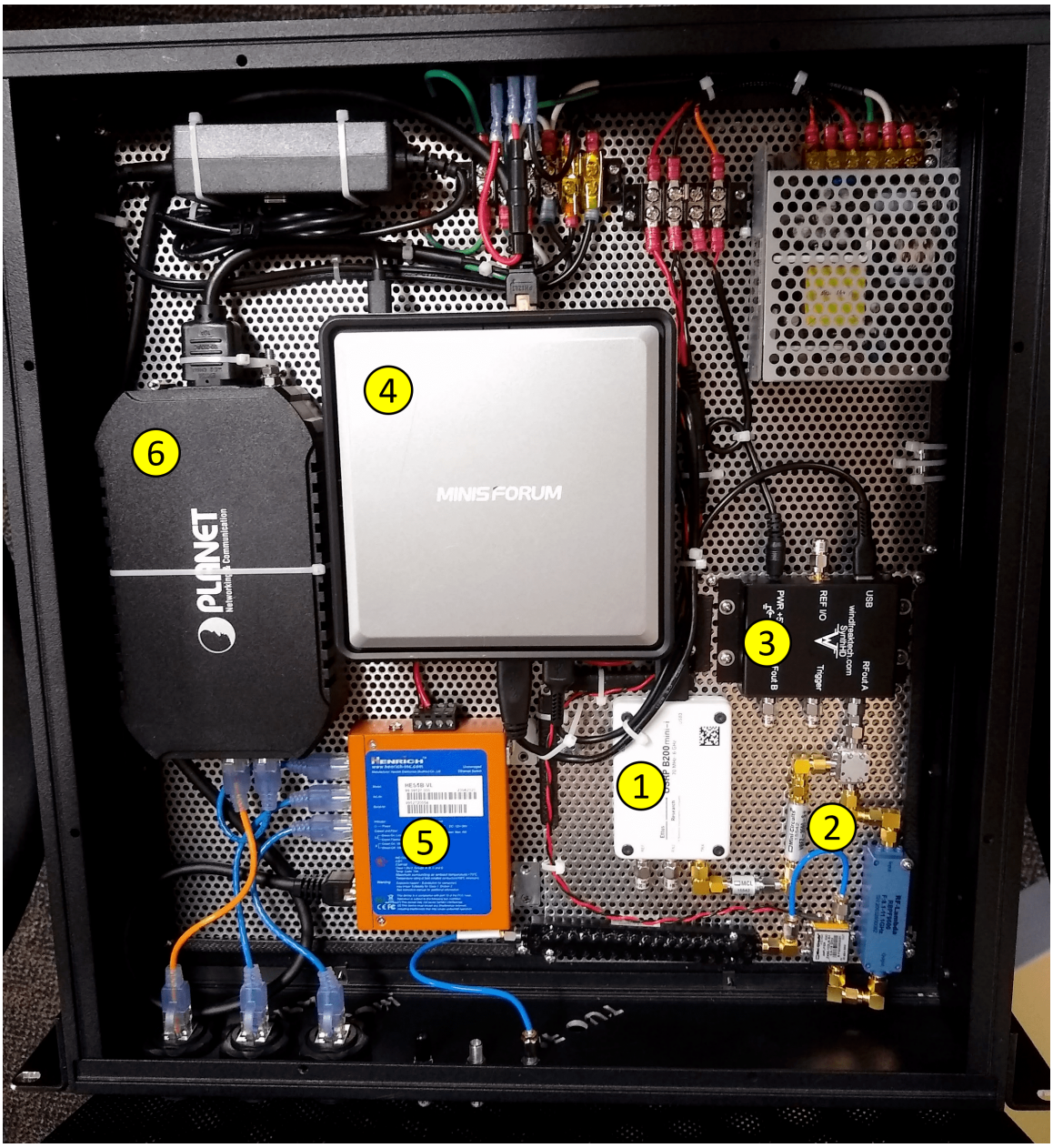

Figure 11: A photo of the components inside System-X's electronics enclosure. Key components are numbered: (1) Ettus B205mini-i SDR (2) X-band upconverter/RFFE (3) Windfreak SynthHD synthesizer (4) Minisforum HM50 (5) Ethernet switch (6) PoE supply.

straightforward to implement upgrades. System-C and System-X's reconfigurability lies in the part of the software that's responsible for waveform generation. In the current version of the GUI, users can specify waveforms by inputting a set of basic parameters that includes modulation type, pulse duration (PD) and PRI (see Section 4.2 for more on waveforms). Once a waveform has been entered into the system, it can be saved in the database for future use.

2.3.7 Electrical Power Distribution

Since System-C/X are designed for use in remote locations, line power will often not be available for use. The power distribution for every subsystems is derived from 120 VAC except for the HPA-C PSU, which takes 240 VAC. The measured power consumption of System-C/X and their major subsystems is listed in Table 7. System-X consumes ~1.4 kW, while System-C consumes a total of ~2.2 kW. These values assume that the electronics enclosure cooler is running, which will depend on the internal temperature of the enclosures at any given time. The power requirements of each system can be supported by gas powered generators with capacities of a few kilowatts. A higher capacity generator can support continuous operation of 12 hours or more.

2.3.8 System-C/X Subsystem Interfaces

The diagrams in Figure 12 and Figure 13 show the subsystem interfaces, types and connections that users of the system will likely need to configure during the life

Power Consumption (W)	System-C	System-X
Electronics box	56 W	74 W
Electronics cooler	400 W	400 W
HPA-Chiller	541 W	368 W
HPA	1200 W	577 W
Total	2197 W	1419 W

Table 7: The approximate power consumption of System-C/X.

of the system. These interfaces include AC and DC power, RF signals, data and communication links, and coolant paths.

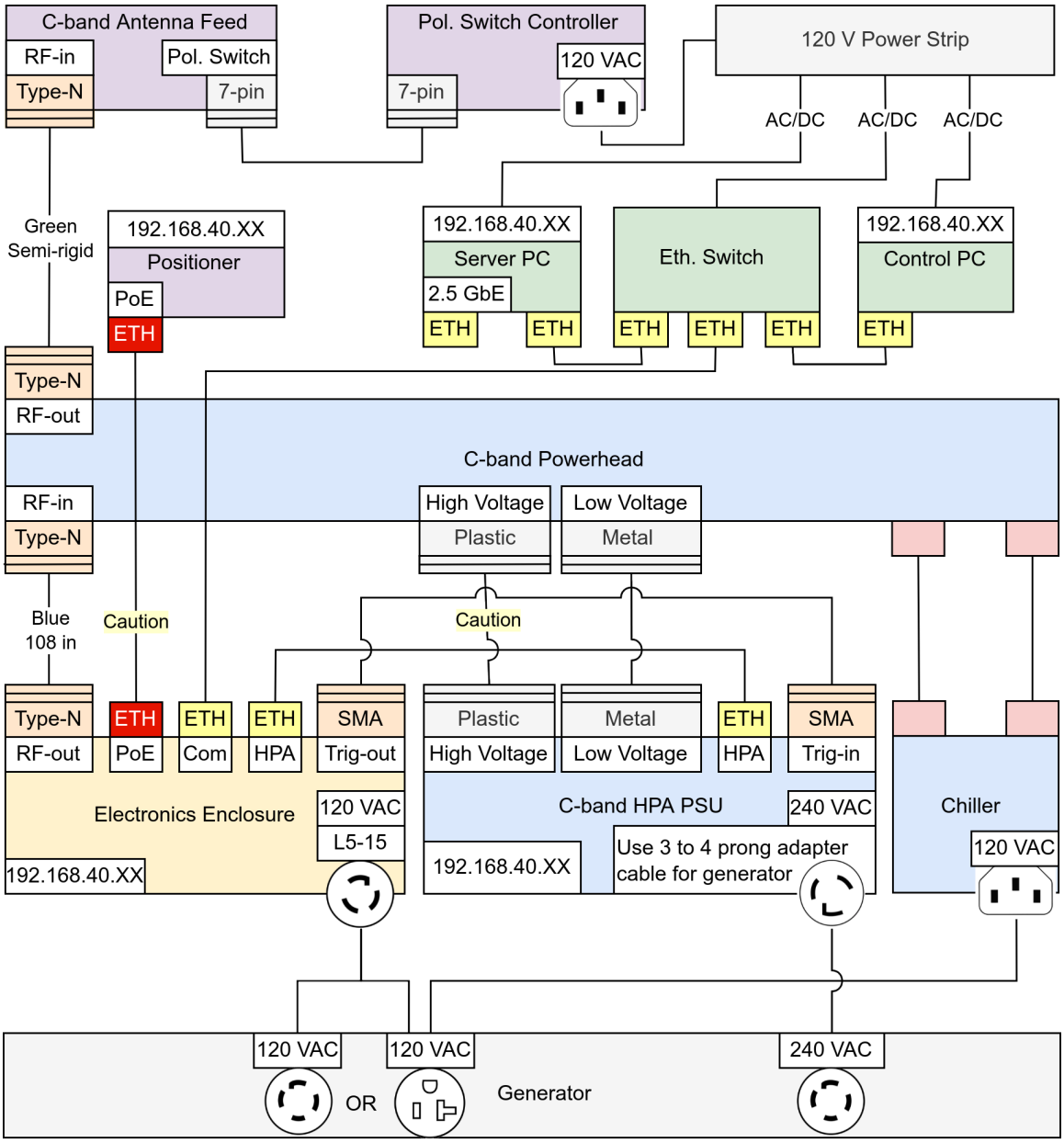

Figure 12: System-C subsystem interfaces diagram.

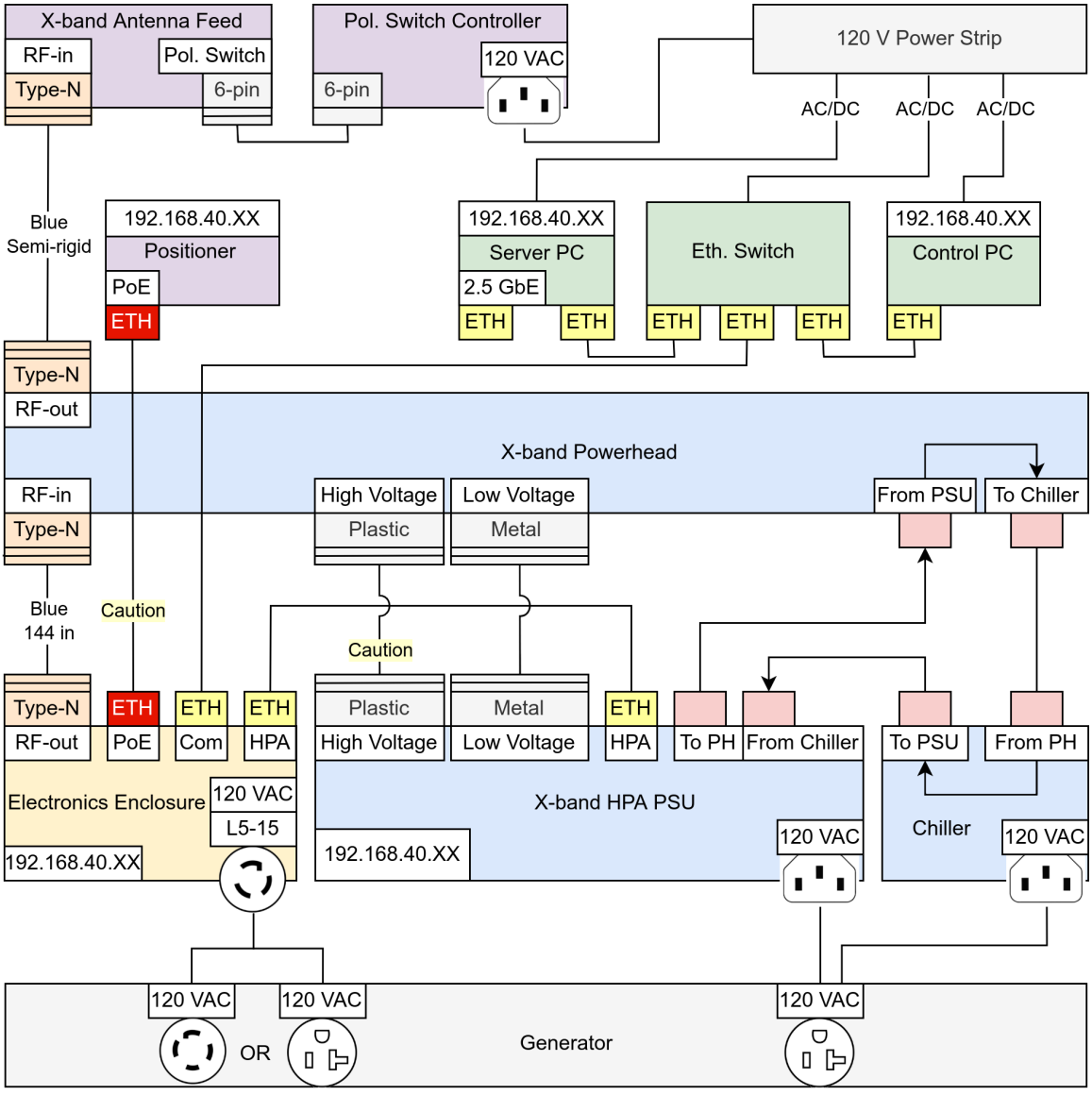

Figure 13: System-X subsystem interfaces diagram.

Chapter 3

DEVELOPMENT

This chapter focuses on various aspects of the HPA-C/X development process.

3.1 HPA Gain Compensation

The CONOPS for System-C/X requires that the two systems produce their maximum possible EIRP over their respective operational bands (3–6 GHz and 8–11 GHz). The HPAs produce their maximum output power when they're driven at their saturation point (see, e.g., Pozar (2011)). As the amplifiers are driven further into saturation, harmonic and non-harmonic distortion increase, the gain starts to decrease, and damage can occur. Therefore, the peak input power to the HPAs is adjusted to correspond to the output saturation power of the amplifiers (these powers are 56 dBm and 49 dBm for System-C/X, respectively).

To drive the HPAs at the proper input level at each carrier frequency, the front end gain of the SDRs is adjusted in software to compensate for the individual frequency responses of each RF component in the signal path. For a two-port device, the frequency response is equivalent to the S_{21} scattering parameter (Pozar (2011)). The process of calibrating out the unwanted frequency response contributions of one or more components in the signal path is sometimes referred to as applying a transfer function correction (see, e.g., Gordon (2019)).

For HPA-C/X, the required gain offset at each carrier frequency is the difference between the input saturation level and the level that's produced at the input to the

HPA using a fixed gain setting in the SDR front end. To be able to compute the gain offsets requires a measurement of the input saturation level as a function of frequency as well as the frequency response of the input signal path. The HPAs' input saturation levels were provided by Quarterwave, in steps of 100 MHz. This data set was then interpolated by a factor of 100. The resulting 1 MHz increment was deemed to be granular enough to support the CONOPS.

The frequency response of each HPA's input signal path was measured by stepping the carrier frequency in 100 MHz increments across the 3 GHz operational bands and recording the peak power at each frequency on a spectrum analyzer. The measured HPA input frequency responses for System-C/X are shown in Figure 14a and Figure 14b, respectively. The frequency response for the System-C signal path varies by more than 10 dB over the operational band, while the System-X signal path varies by $\sim$6 dB. The variation of several dB over hundreds of megahertz is in part due to the long (10–12 ft) coaxial cables that are used in the signal path.

The input saturation levels for HPA-C/X are shown as a function of frequency in steps of 100 MHz (blue traces) in Figure 15a and Figure 15b. There is a large variation in power in both curves (>10 dB for HPA-C and >7 dB for HPA-X). Whereas the input saturation power increases with frequency for HPA-C, it decreases with frequency for HPA-X.

Because the goal of the gain calibration is to make the curves in Figure 14 match the blue traces in Figure 15, the gain offsets that should be applied to the SDR front end at each frequency are found by taking the difference between the two curves. The result of applying the gain offsets is shown in the red traces in Figure 15a and Figure 15b. After applying a DC offset to the correction so that absolute power

levels match up, the frequency responses for both systems (red traces) match the target input levels (blue traces) to within 1 dB.

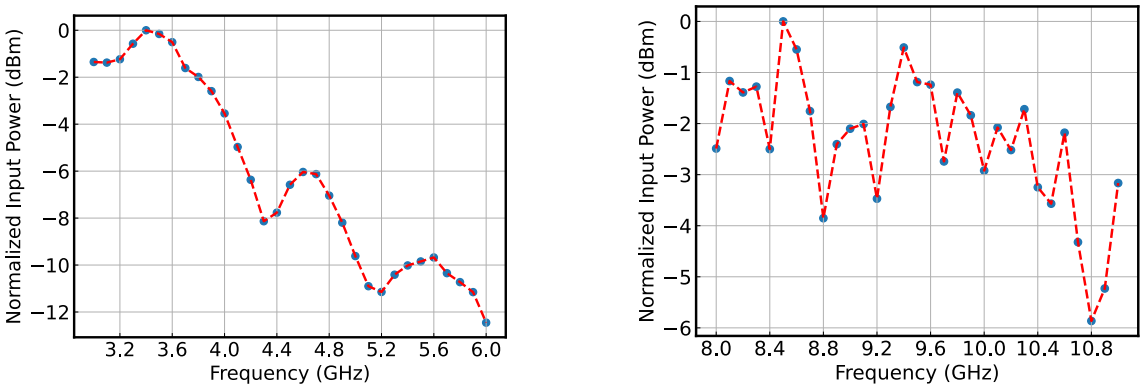

(a) (b)

Figure 14: (a) The uncorrected frequency response of the HPA-C input chain (b) The uncorrected frequency response of the HPA-X input chain.

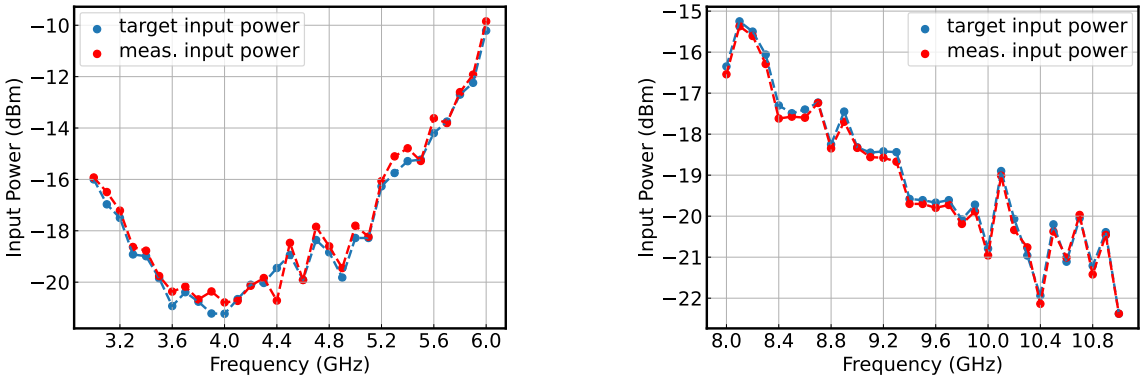

(a) (b)

Figure 15: (a) HPA-C input saturation levels (blue) and corrected HPA input power levels (red) (b) HPA-X input saturation levels (blue) and corrected HPA input power levels (red).

After applying the computed gain offsets to the SDR front ends of each system, the peak output power that's produced by the HPAs should be close to their target

output saturation levels. Figure 16a and Figure 16b show measurements of the output power for each HPA that corresponds to the input levels shown in Figure 15. To take this measurement, the output of the HPAs was connected to a 30 dB coupler, and the power output from the coupler was further attenuated before being connected to the input of a spectrum analyzer using a long cable run. To extract the true output power levels of the HPAs, the frequency response of each element in the coupler signal path (including the coupler itself) was measured using a vector network analyzer and subtracted from the total.

For HPA-C, the variation of $\sim$2 dB across the 3–6 GHz band is a significant improvement over the $>$ 10 dB variation in the input saturation levels shown in Figure 15a. In this measurement, the overall gain has been lowered by $\sim$1 dB so that the output power stays at or below 56 dBm over the majority of the operational band. Figure 16b shows the measured output power for HPA-X that corresponds to the input saturation levels in Figure 15b. The frequency response is flat to within $\sim$1.5 dB. As was done with HPA-C, the overall gain has been lowered by 1–2 dB to prevent the HPA from being driven too far into saturation. The residual gain variations in the measurements shown in Figure 16 can be attributed to imperfections in the measurement calibration and to variations in the gain characteristic of the HPAs.

3.1.1 Gain Coefficient Interpolation

The SDR gain offsets are stored in a look-up-table (LUT) onboard the client PCs that can be accessed by the client software. These offsets are calculated from RF measurements that were taken at 100 MHz steps. To allow for the offsets to be applied to any user-specified frequency (within the limits of the system), the values in

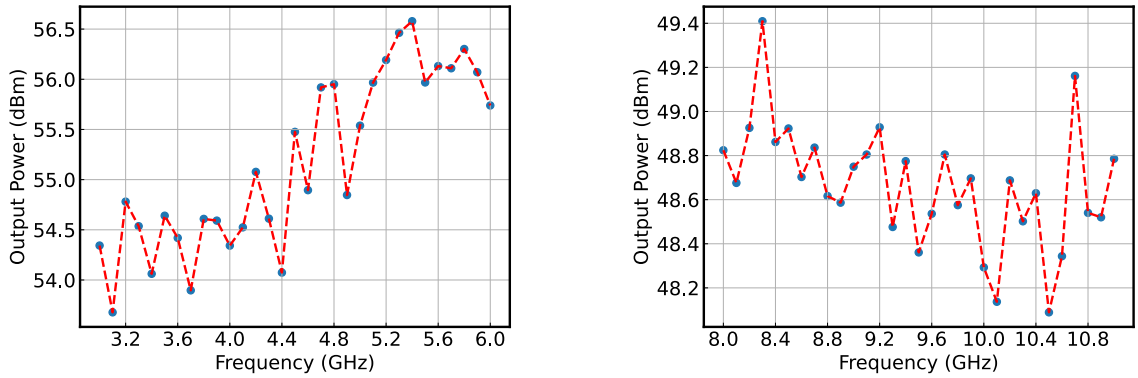

(a) (b)

Figure 16: (a) HPA-C output saturation power as a function of frequency (b) HPA-X output saturation power as a function of frequency.

the LUT are interpolated by a factor of 100 using a cubic spline. When a user specifies a waveform carrier frequency, the SDR software selects the gain offset corresponding to a frequency that's at most 500 kHz from the desired frequency.

3.2 Harmonic Distortion

Since the operational band of HPA-C is one octave (3–6 GHz), low frequency carriers can affect the linearity and output power of the TWT. The second harmonic has the highest potential to cause problems. Although HPA-C contains a LPF at the TWT output, the second harmonic can not be completely eliminated when using carrier frequencies in the lower part of the operational band. Additionally, at drive levels approaching the input saturation level, the second harmonic increases the thermal load on the output LPF, which leads to gain reduction and changes in frequency response.

Figure 17a shows a spectrum analyzer measurement of the HPA-C output for an input tone at 3.0 GHz. The second harmonic at 6 GHz is ~15 dB down from the

3 GHz fundamental. Since the measurement has not been corrected for the influence of the HPA output coupler, attenuators and cabling that were used in the test setup, the second harmonic level is significantly higher than what is shown in Figure 17a.

Figure 17b shows the power in the second harmonic (in dBc) in steps of 10 MHz for the first ~40 MHz of the 3–6 GHz band. As in Figure 17a, this data is not calibrated, and the second harmonic levels that are shown represent lower limits. The true levels could be up to 3 dB higher than those shown in Figure 17b.

One way to mitigate the effects of the second harmonic would be to use an output LPF with a narrower transition band. The currently installed filter is a COTS component. In a future version of System-C, a custom output LPF could be used instead.

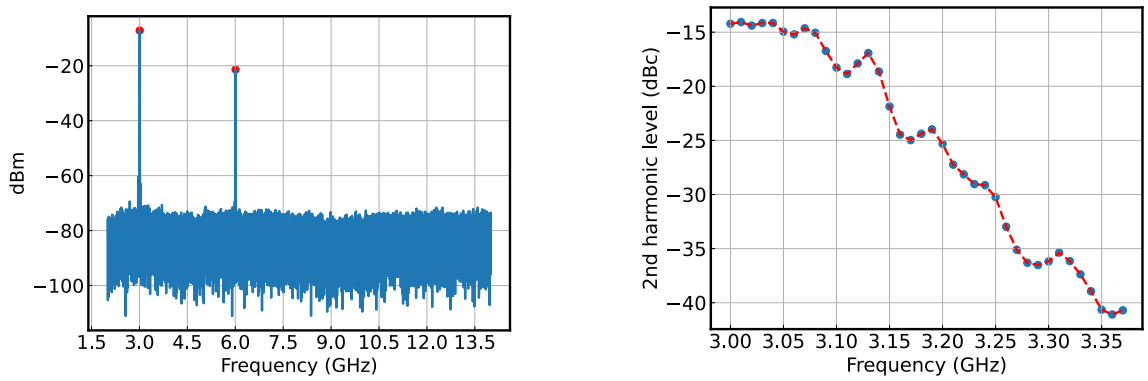

(a) (b)

Figure 17: (a) A spectrum analyzer trace showing the HPA-C output for an input tone at 3 GHz (b) The output power in the second harmonic relative to the fundamental signal input to HPA-C.

3.3 HPA-C Gating System

As mentioned in Section 2.3.1.2, the HPA-C TWT must be turned off (gated) during the dwell times for pulsed waveforms to minimize the power dissipation inside the RF powerhead. To ensure that the gating occurs at the right times, it must be triggered by an external signal. In System-C, the gating trigger signal is generated using the second channel of the N300 USRP.

The gating trigger signal is a pulsed tone at the carrier frequency of the RF signal (the carrier frequency of the gating signal is not critical) with a PRI that matches that of the RF signal that's generated using the other TX channel. The gating trigger signal is input to the HPA-C PSU via an SMA port that feeds it to an envelope detector circuit. After the circuit has rectified the waveform to produce the envelope, the envelope is converted to a TTL signal that a MCU uses to control the actual gating voltage.

For the TWT gating system to work as intended, the amplitude of the gating signal must be properly matched to the input of the envelope detector circuit. This is achieved by applying a similar gain correction to the one described in Section 3.1.

In addition to controlling the amplitude of the gating trigger signal, it's critical to control the relative time delay between the gate and RF signals. Whereas the RF signal that's produced by the N300 goes directly to the RF powerhead and TWT, the gating trigger signal enters the PSU and triggers a series of events that must occur before the TWT is gated. Therefore, the rising edge of the gating trigger signal must lead the rising edge of the RF signal by some amount of time.

The gating signal delay was determined by inputting an RF signal with a fixed PRI to HPA-C while monitoring the amplified output signal on an oscilloscope. When

the lead time for the gating signal is too short, the TWT gets cut off before the end of the RF pulse, and the RF pulse is truncated in time. To determine the right lead time, RF pulses were observed on an oscilloscope while the delay was increased in small time increments. A lead time of 1 μs was found to result in clean RF pulses. The 1 μs lead time was used with additional PRIs to ensure that it worked well across the parameter space.

The 1 μs delay between the gating and RF signal means that from the point of view of the TWT, the effective PD is at least 1 μs longer than the PD of the stimulus. Therefore, the waveform PRI is limited to $\lesssim 1$ μs. Figure 18 shows an oscilloscope screen capture of the rising edge of the gating trigger signal (green trace) compared to that of the RF signal (yellow trace) for a single pulse. The measurement was taken from the output of the N300, and serves to demonstrate the 1 μs delay between each set of pulses.

Figure 18: An oscilloscope capture of the rising edges of a HPA-C gating pulse (green) and signal pulse (yellow).

Chapter 4

TESTING

The following sections describe the testing methodology that was used to verify that System-C/X produce peak EIRPs of $\gtrsim 50$ dBW over their operational bands. Section 4.1 describes the test range and testing configuration. Section 4.2 discusses the waveforms that were used during the tests. Section 4.3.2 explains the link budget and parameters that were used to estimate the EIRP of the two systems. EIRP estimates are presented in Section 4.3. Finally, Section 4.4 presents beam pattern measurements for System-C/X.

4.1 System-C/X Test Configuration

The test range that was used for broadcasting is located at mWAVE Industries' headquarters in Windham, Maine. The measurements presented in the following sections were taken during a System-X test in July 2021 and a System-C test in January 2022. FCC approval to broadcast each test waveform was acquired prior to all testing events.

The usable length of the test range is $\sim$130 m. A receiver platform is placed at one end of the range while the tests are conducted from the opposite end. The receiver is a 0.6 m dish that can be coupled to one of several feed horns. The receiver boresight is at a height of $\sim$6 m. The length of the range allows for System-C/X to be positioned such that the receive antenna is located in the far-field of the transmitter beams (distances of $\sim$34 m and $\sim$62 m, for System-C/X). Figure 19 shows a view of

the test range taken in July 2021 from behind System-C, facing the receiver platform. Figure 20 shows a similar view, taken at the second field test in January 2022. The receiver platform and structures around it (as well as the ground) have the potential to cause reflections and multipath effects during each transmission (Balanis (2015)).

Prior to the start of testing, the transmitter and receiver antenna boresights were aligned. The alignment was achieved by driving the transmitter with a CW signal while scanning in azimuth and elevation and recording beam patterns with a dedicated system that's operated by mWAVE.

Figure 19: System-C at the test site in July 2021.

Figure 21 shows a simplified diagram of the test setup that was used for System-C.

Figure 20: System-C at the test site in January 2022.

The transmitter and receiver were separated by 39 m. Switching between horizontal and vertical polarizations (H-pol and V-pol) was done with an electronic switch on the transmitter feed and a manual switch on the receiver feed (these switches are not shown in the diagram). Two different receiver feed horns were used during the test, one for the lower and upper parts of the band. These feeds were switched out between transmissions.

Figure 22 shows a simplified diagram of the test setup that was used for System-X. The transmitter and receiver were separated by 76 m. Switching between H-pol

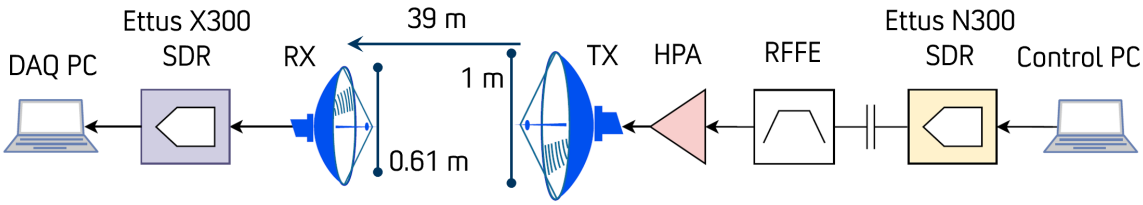

Figure 21: The test configuration for System-C.

and V-pol was done in the same manner as for System-C. A single receiver feed horn was used during the test.

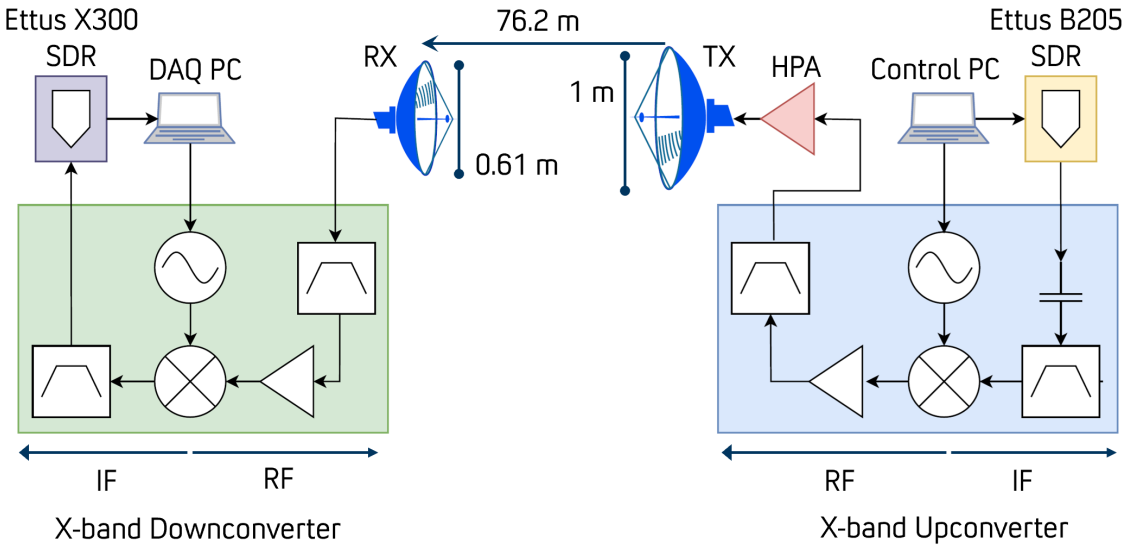

Figure 22: The test configuration for System-X.

4.1.1 Data Acquistion System

A data acquisition (DAQ) system was devised for both the System-C/X tests to allow for recording raw I/Q data during the test transmissions (for a detailed overview of quadrature signal processing, see Lyons (1997)). The data recording systems consists of an Ettus X300 USRP and a laptop computer with a large amount of data

storage. For System-X, a X-band downconverter was constructed to downconvert the received waveforms to the IF band of the X300 (∼DC–6 GHz). During the tests, the DAQ system was located on the receiver platform below the receiver dish. A series of coaxial cables and attenuators were used to couple the output of the receiver feed to the SMA input connector on either the downconverter (for System-X), or the X300 (for System-C). The DAQ was remotely controlled from the transmitter position down-range from the receiver, and 0.1–1 s frames were recorded during each transmission.

The raw I/Q data recorded by the DAQ system is stored in analog-to-digital converter (ADC) counts. Each I/Q sample is a pair of 16-bit two's complement integers, with a maximum ADC count of 32767 (Smith et al. (1997)). To be able to estimate the peak power at the receiver, the ADC counts must be calibrated into an equivalent peak power in units of dBm. This calibration was performed by generating a tone for each of the IF carrier frequencies (3.5 GHz for System-X, 3.256 GHz and 4.756 GHz for System-C) and inputting it to the X300 system. The tone power was increased until the peaks of the digitized waveform clipped (this occurs when the ADC count is 32767). The tone power that produces a maximum count of 32767 in the digitized waveform is taken to be the full-scale input power P_{FS} of the X300. Knowing P_{FS} for a particular carrier frequency allows the raw I/Q values to be converted to a peak power:

$$P_{ADC} \simeq P_{FS} - 20\log_{10}\left(32767/\sqrt{I^2+Q^2}\right) \qquad \text{(dBm)} \quad (4.1)$$

Equation 4.1 is used to assign a peak input power to each data capture.

4.2 Test Waveforms

The test waveforms for System-C/X were selected to ensure that the two systems would be evaluated under an adequate range of operational conditions. For each system, three carrier frequencies were chosen to correspond to the middle, lower and upper regions of the operating band. For System-C, only the two lower frequencies were approved for testing. The approved carrier frequencies are 3.256 GHz and 4.756 GHz for System-C, and 8.706 GHz, 9.506 GHz and 10.906 GHz for System-X. In the following, each carrier frequency is denoted by the letter *c*, followed by a number, and the corresponding band (e.g., c1-c, for System-C's first carrier frequency). The maximum IBW used for the test waveforms is 12 MHz. The carrier frequencies used for System-C/X are listed in Table 8 with their corresponding identifiers and maximum allowable IBWs.

System	Carrier Identifier	Carrier Frequency (GHz)	IBW max. (MHz)
C	c1-c	3.256	12
C	c2-c	4.756	12
X	c1-x	8.706	12
X	c2-x	9.506	12
X	c3-x	10.906	12

Table 8: Test carrier frequency identifiers and parameters.

For the EIRP test described in Section 4.3, three different waveforms (wf1–wf3) were tested at each carrier frequency, in both horizontal and linear polarization states. These parameter combinations yield a total of 12 different waveform combinations for System-C and 18 combinations for System-X. The modulation type, PD, PRI and duty cycle for the three test waveform types are listed in Table 9. Waveform-1 (wf1)

is an unmodulated pulse with a 1 μs PD and 10% duty cycle. Waveform-2 (wf2) is a LFM chirp with a wide PD of 60 μs and a duty cycle of 30%, and waveform-3 (wf3) is a BPSK (binary phase-shift keying) waveform with a PD of 10 μs and duty cycle of 10%. Unmodulated pulses and LFM chirps are commonly used radar waveforms, while BPSK is used in both radar and communications applications (see, e.g., Bliss (2021), Stimson (2014), Sklar (2001)).

Individual test waveforms are referenced using their waveform and carrier identifiers (e.g., waveform-1 using the lowest carrier frequency for System-C is wf1-c1-c).

Waveform Identifier	Modulation	PRI (μs)	Pulse Duration (μs)	Duty Cycle (%)
wf1	Pulsed	10	1	10
wf2	LFM	200	60	30
wf3	Random BPSK	100	10	10

Table 9: Test waveform identifiers and parameters.

4.3 Estimating the Peak EIRPs for System-C/X

From the standpoint of the transmitters, the EIRP is calculated as:

$$\text{EIRP} = 10\log_{10} P_{\text{TX}} + 10\log_{10} G_{\text{TX}} \qquad \text{(dBW)} \quad (4.2)$$

where P_{TX} is the transmitted power in watts, and G_{TX} is the transmit antenna gain $G_{\text{TX,ant}}$ in dBi, minus any losses from cables and other passive components in the transmit signal path (Huang (2021)).

4.3.1 Sources of Uncertainty in the EIRP Estimates

The EIRP of the two systems can't be measured directly, and there are several uncertainties associated with the measurement. On the transmit side, it's possible that both the output power of the HPAs and the antenna gain are different from their assumed values due to an imperfect impedance match between the output of the HPA and input of the antenna feed (Pozar (2011)).

On the receiving end of the system, the primary uncertainty is the receiver efficiency at each carrier frequency. In the following analysis, a constant efficiency of 38% is assumed for all carrier frequencies[8].

As mentioned in Section 4.1, the test setup for System-C/X is prone to multipath interference resulting from reflections from the ground, receiver platform and structures that are close to the receiver. While multipath effects are not modeled in this analysis, it is assumed that they are related to some features that are observed in the beam pattern measurements presented in Section 4.4 (for a detailed discussion of antenna testing and analysis, see Balanis (2015)).

Given the set of measurement uncertainties described above, it's expected that the EIRP estimates will only be accurate to within $\sim$3 dB of their true values.

4.3.2 Link Budget Calculations

This section presents a link budget that can be used to relate the EIRP of Equation 4.2 (which must be estimated) to the peak power P_{RX} that will be measured at the output of the receiver feed using the DAQ system. The received power can

[8]This value was provided by mWAVE in a private communication

be estimated using the Friis transmission formula (also known as the one-way radar equation) (see, e.g., Friis (1946), Skolnik (1980), Center (1997)),

$$P_{\mathrm{RX}} = \frac{P_{\mathrm{TX}} G_{\mathrm{TX}} A_e}{4\pi d^2} \quad \text{(W)} \quad (4.3)$$

where A_e is the effective area of the receiver dish and d is the distance between the transmit and receive antennas. The effective area of the receiver dish is calculated as $A_e = A\epsilon_r$, where A is the geometric area and ϵ_r is the efficiency of the receiver (the product of the aperture and radiation efficiencies). For the receiver used in this measurement, $\epsilon_r = 38\%$.

By expressing A_e in terms of the receiver gain and carrier wavelength λ: ($A_e = \frac{G_{\mathrm{RX,ant}}\lambda^2}{4\pi}$), Equation 4.3 can be rewritten as

$$\begin{aligned} P_{\mathrm{RX}} &= P_{\mathrm{TX}} G_{\mathrm{TX}} G_{\mathrm{RX}} \left(\frac{\lambda}{4\pi d}\right)^2 \\ &= P_{\mathrm{TX}} G_{\mathrm{TX}} G_{\mathrm{RX}} \left(\frac{c}{4\pi d f_c}\right)^2 \end{aligned} \quad \text{(W)} \quad (4.4)$$

where c is the speed of light and f_c is the carrier frequency. The ratio in parenthesis in Equation 4.4 is the inverse of the free-space path loss (FSPL):

$$\mathrm{FSPL} = \left(\frac{4\pi d f_c}{c}\right)^2 \quad (4.5)$$

Taking the log of Equation 4.4 yields a simple expression for P_{RX}:

$$P_{\mathrm{RX}} = 10\log_{10}(P_{\mathrm{TX}}) + 10\log_{10}(G_{\mathrm{TX}}) + 10\log_{10} G_{\mathrm{RX}} - \alpha \quad \text{(dBW)} \quad (4.6)$$

where $\alpha = 10\log_{10} FSPL$:

$$\alpha = 20\log_{10}(d) + 20\log_{10}(f_c) + 20\log_{10}\left(\frac{4\pi}{c}\right) \quad \text{(dB)} \quad (4.7)$$

In the above expressions, G_{TX} and G_{RX} represent their respective antenna gains in addition to any losses in the signal path of the transmitter and receiver.

4.3.3 EIRP Estimation Method

This section provides an example of how the EIRP is estimated from each transmission measurement. The test waveform is an unmodulated pulse with $f_c =$ 8.706 GHz, $PD = 2$ µs and $PRI = 20$ µs. The polarization is H-pol. Figure 23 shows the raw I/Q ADC counts for a single pulse of the waveform that was recorded using the DAQ SDR (top frame) and the phase of I and Q (bottom frame). The spectrum of the pulse is shown in Figure 24.

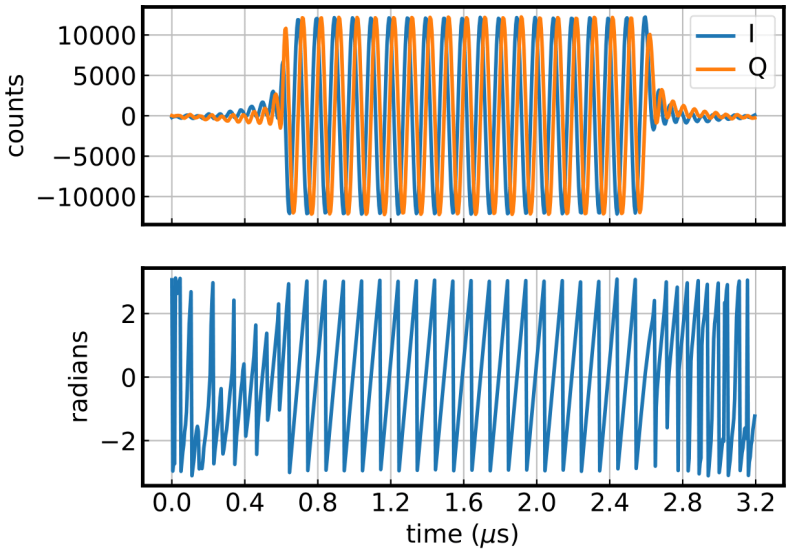

Figure 23: I/Q counts and phase for a single pulse of the example waveform.

Table 10 lists values for the link budget parameters for this waveform, rounded to one decimal place. The values in the second column of Table 10 are estimated

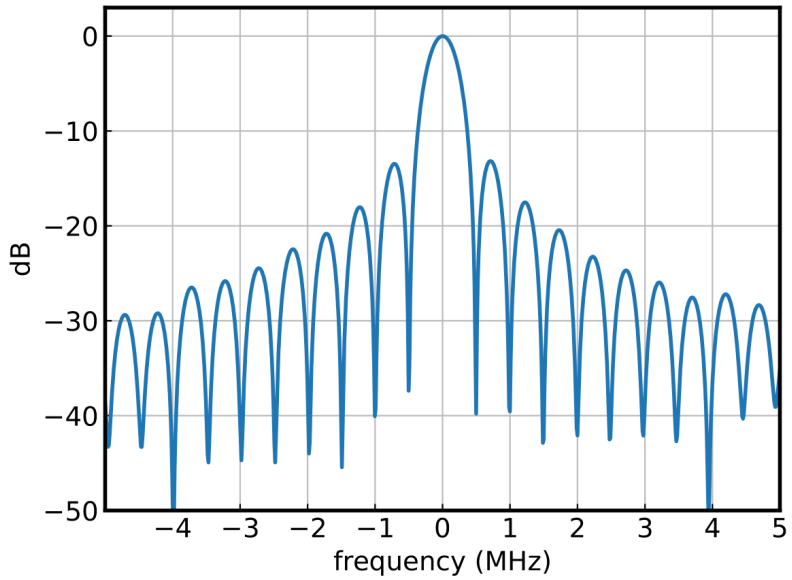

Figure 24: The spectrum of the example test waveform.

Parameter	Est.	Meas.	Note
P_{TX} (dBm)	49.9		
G_{TX} (dBi)	34.9		
α (dB)	88.9		
G_{RX} (dBi)	-12.0		
P_{RX} (dBm)	-16.1	-19.0	Peak power at SDR input
$EIRP$ (dBW)	56.2	53.4	Meas. value corresponds to P_{RX} meas.

Table 10: The estimated and measured link budget parameters for wf1-c1-x.

from a combination of direct measurements (e.g., measurements of the HPA output power) and assumed parameters (e.g., the antenna gains of the transmitter and receiver). These values suggest that the EIRP for this waveform should be ∼56 dBW, and that the peak power received at the DAQ SDR should be ∼-16 dBm. The peak power that was actually measured at the DAQ SDR is -19 dBm. This suggests that the actual EIRP is closer to ∼53 dBm.

Given the available information, it's not possible to know the exact source of

the discrepancy between the two EIRP estimates. While either value (or their mean) could be adopted as the assumed EIRP, for the purposes of this document the EIRP that corresponds to the SDR peak power measurement is taken as the EIRP for each test transmission.

4.3.4 System-C/X EIRP Estimates

Peak EIRP estimates for each of the System-C/X test waveforms are shown in Figure 25a and Figure 25b, respectively. The EIRP values are listed in Table 11. All values are within ∼3 dB of the target peak EIRP of ∼50 dBW.

For both systems, the highest estimated EIRPs correspond to the highest carrier frequency (4.756 GHz for System-C and 10.906 GHz for System-X). This is expected, because the transmit antenna gain increases with frequency (at least over the design passbands). It was observed that very similar (to within ∼0.5 dB) EIRPs are produced for the same waveform in each polarization.

The most notable feature in System-X's EIRP data is that the 9.506 GHz waveform EIRPs are ∼3 dB lower than those for the other two carriers. The frequency response of HPA-X is one possible source of the EIRP discrepancy. Because the HPA-X data presented in Section 3.1 corresponds to a different TWT than the one that was used for the EIRP measurements, this hypothesis can't be tested.

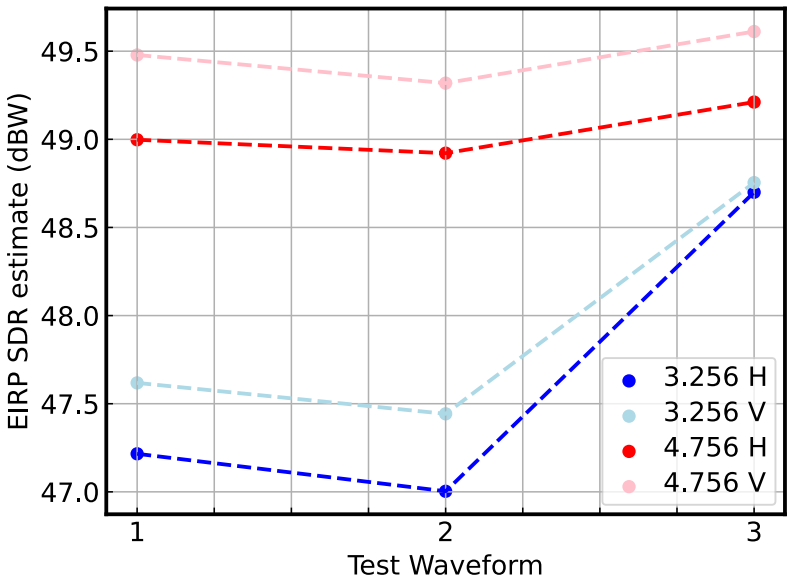

(a)

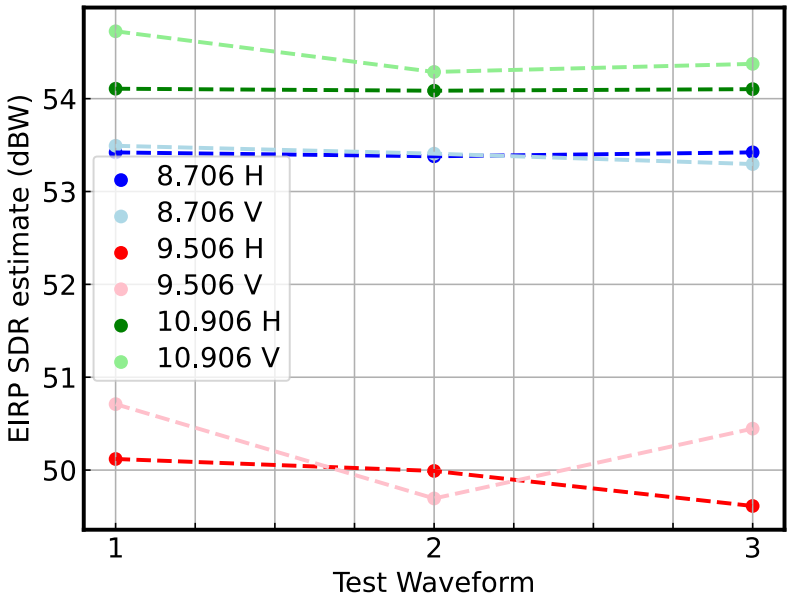

(b)

Figure 25: (a) EIRP estimates for the System-C test waveforms (b) EIRP estimates for the System-X test waveforms.

Waveform	$EIRP_{est,H}$ dBW	$EIRP_{est,V}$ dBW
wf1-c1-c	47.2	47.6
wf2-c1-c	47.0	47.4
wf3-c1-c	48.7	48.8
wf1-c2-c	49.0	49.5
wf2-c2-c	48.9	49.3
wf3-c2-c	49.2	49.6
wf1-c1-x	53.4	53.5
wf2-c1-x	53.3	53.4
wf3-c1-x	53.4	53.3
wf1-c2-x	50.1	50.7
wf2-c2-x	50.0	49.7
wf3-c2-x	49.6	50.4
wf1-c3-x	54.1	54.7
wf2-c3-x	54.1	54.3
wf3-c3-x	54.1	54.3

Table 11: Estimated peak EIRPs for System-C/X.

4.4 Beam Pattern Measurements

This section presents beam pattern measurements that were taken for System-C/X at the mWAVE test range during the same test events discussed in previous sections. The primary objective of these measurements is to verify that the main beam widths of antenna-C/X are close to their design HPBWs of ∼6 deg and ∼3 deg (these values depend on the carrier frequency). A secondary objective is to evaluate the level of the first sidelobe. This second objective is complicated by the presence of multipath effects that for the purposes of these tests were not quantified.

The test configuration for the beam pattern measurements is the same as the one that was used for the EIRP measurements. All beam patterns for both systems were acquired using wf1 (the unmodulated pulse) as the stimulus. The patterns for each

system are presented as azimuth and elevation crosscuts for both polarizations. To produce an azimuth crosscut, the antennas were stepped in regular intervals (generally of 0.5–1 deg) while the elevation coordinate was held constant. The elevation crosscuts were taken using the same method, except that the antenna azimuth was held constant while the elevation was stepped. To avoid causing significant ground reflections, the transmit antenna elevations were never lowered below the boresight of the receive antenna.

Table 12 lists the measured HPBWs for each crosscut measurement, with the corresponding carrier frequency and polarization. The measurements are shown in Figure 26–Figure 29, where V-pol is shown in pink and H-pol is shown in blue. The magnitude of the two traces in each figure is shown normalized to the maximum value of the pair.

4.4.1 Antenna-C Beam Patterns

Figure 26a and Figure 26b show the azimuth and elevation crosscuts for the 3.256 GHz and 4.756 GHz carrier frequencies. The median HPBW for all of the 3.256 GHz crosscuts is ~7.2 deg. At 3.256 GHz the first sidelobe is clearly visible in all measurements. The overall sidelobe levels relative to the main beam are close to those found in a series of reference measurements that were provided by mWAVE. There's a sharp discontinuity in the 3.256 GHz H-pol azimuth crosscut that occurs between -3 deg and -6 deg. This feature is assumed to be due to a measurement error with the DAQ system.

The 4.756 GHz crosscuts are shown in Figure 27a and Figure 27b. The median beamwidth is 5.4 deg. The first sidelobe is clearly visible in the V-pol azimuth and

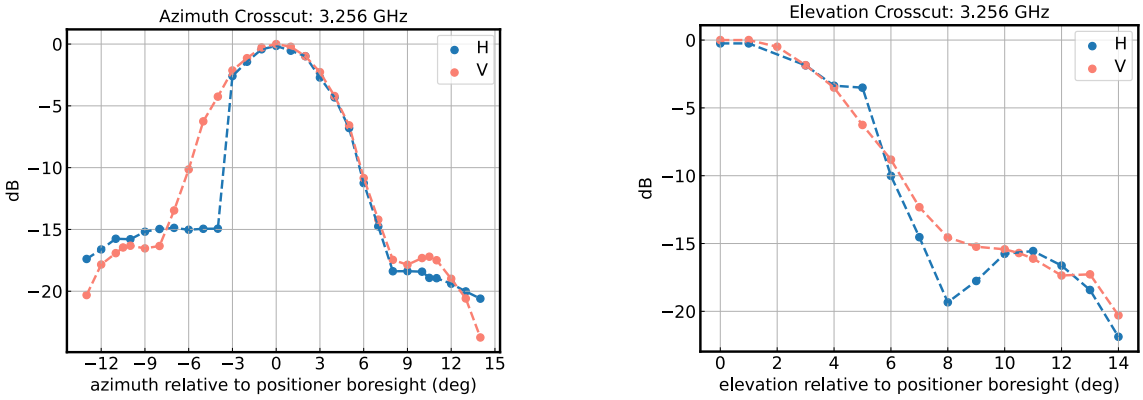

(a) (b)

Figure 26: (a) Azimuth crosscuts for antenna-C at 3.256 GHz in V-pol and H-pol (b) elevation crosscuts for antenna-C at 3.256 GHz in V-pol and H-pol.

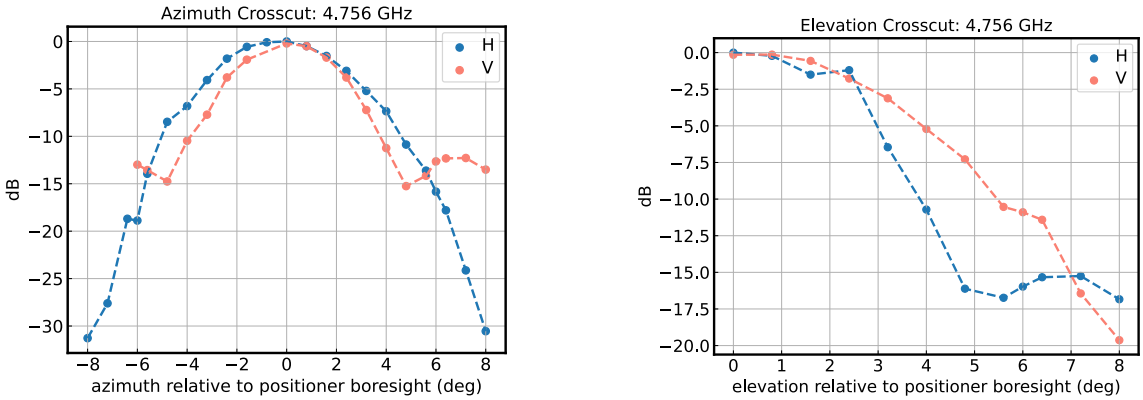

(a) (b)

Figure 27: (a) Azimuth crosscuts for antenna-C at 4.756 GHz in V-pol and H-pol (b) elevation crosscuts for antenna-C at 4.756 GHz in V-pol and H-pol.

H-pol elevation crosscuts, but is less pronounced in the H-pol azimuth and V-pol elevation crosscuts. This is thought to be an effect of the multipath interference from the ground and structures around the receiver platform.

4.4.2 Antenna-X Beam Patterns

System-X beam pattern measurements were taken at 8.706 GHz and 10.906 GHz. Figure 28a and Figure 28b show the 8.706 GHz azimuth and elevation crosscuts. The median HPBW is ∼2.1 deg.

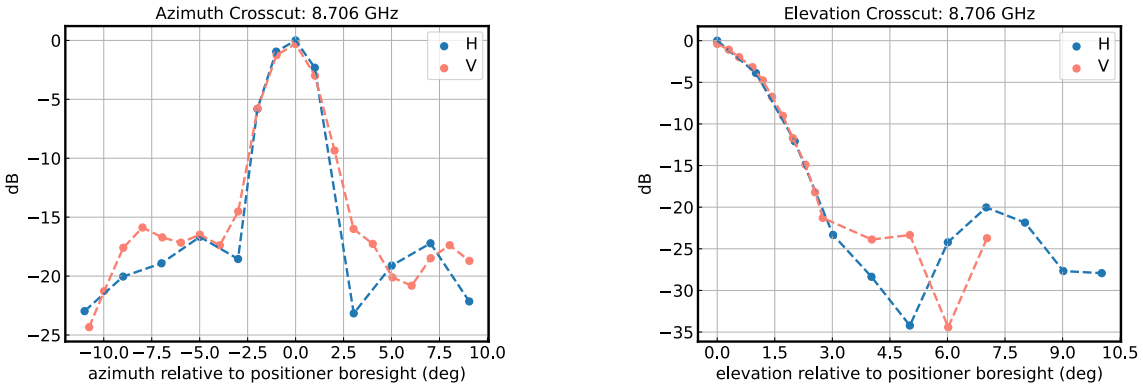

(a) (b)

Figure 28: (a) Azimuth crosscuts for antenna-X at 8.706 GHz in V-pol and H-pol (b) elevation crosscuts for antenna-X at 8.706 GHz in V-pol and H-pol.

The 10.906 GHz azimuth and elevation crosscuts are shown in Figure 29a and Figure 29b. Their median HPBW is ∼1.9 deg, which is consistent with the higher frequency.

The first sidelobes are clearly visible in all of the antenna-X beam pattern measurements. The sidelobe levels in the elevation crosscuts are found to be consistent with the levels shown in a set of reference measurements for the same antenna. However, the sidelobe levels in the azimuth crosscuts are found to be ∼10 dB higher than the levels in the reference measurements. The elevated sidelobes in the azimuth crosscuts are again thought to be caused by multipath effects originating in the test configuration.

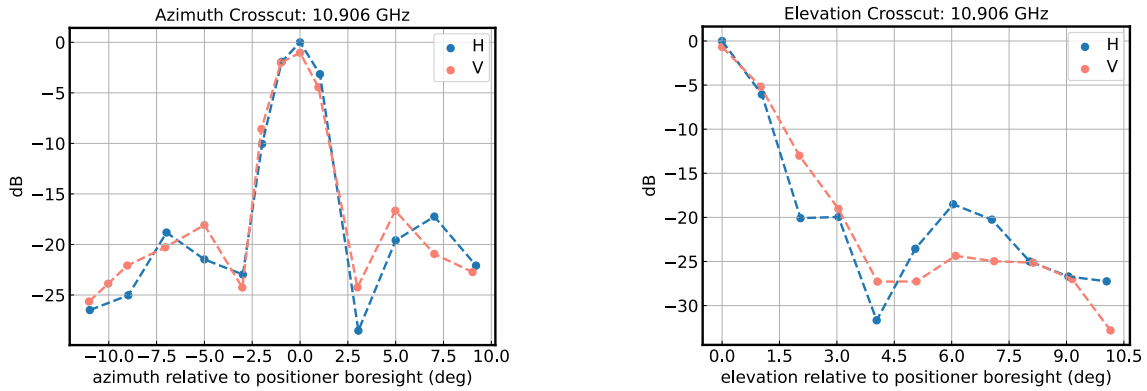

(a) (b)

Figure 29: (a) Azimuth crosscuts for antenna-X at 10.906 GHz in V-pol and H-pol (b) elevation crosscuts for antenna-X at 10.906 GHz in V-pol and H-pol.

System	Carrier Freq. (GHz)	Pol.	Crosscut	HPBW (deg)
C	3.256	H	Az.	6.21
C	3.256	V	Az.	6.83
C	3.256	H	El.	8.96
C	3.256	V	El.	7.51
C	4.756	H	Az.	5.23
C	4.756	V	Az.	4.32
C	4.756	H	El.	5.47
C	4.756	V	El.	6.29
X	8.706	H	Az.	2.73
X	8.706	V	Az.	2.52
X	8.706	H	El.	1.67
X	8.706	V	El.	1.75
X	10.906	H	Az.	2.20
X	10.906	V	Az.	2.06
X	10.906	H	El.	1.69
X	10.906	V	El.	1.39

Table 12: Measured antenna-C/X HPBWs.

Chapter 5

CONCLUSION

The previous chapters presented the design, development and testing of System-C and System-X, two high-power, reconfigurable RF transmitters. Chapter 2 describes the process of translating a simple CONOPS to a set of system requirements. These system requirements are then used to create a system architecture. The final result of the design process is a set of component and subsystem-level specifications that describe each of the systems' capabilities and interfaces.

During the development phase discussed in Chapter 3, System-C/X's hardware subsystems (SDRs, electronics enclosures, HPAs and antennas) are integrated together and tested. This chapter focuses on steps that were taken to fine-tune the gain of the RF systems, and to calibrate the HPA-C gating system.

Chapter 4 describes the field testing that was performed in July 2021 and January 2022 to estimate the peak EIRP of System-C/X at multiple carrier frequencies, and to measure their beam widths. The results of the performance testing show that both systems produce their target peak EIRPs of ≥ 50 dBW to within an acceptable margin of measurement uncertainty. Additionally, System-C/X are found to produce HPBWs that are close to their design values of $\sim$3 deg and $\sim$6 deg.

Now that System-C/X have been shown to function as designed, the question of how their interfaces and performance might be improved in future versions of the systems can be addressed.

5.1 Future Work

From a functionality standpoint, System-C/X could be improved by simplifying the interfaces between the various subsystems. In the current version, each system has a total of six cables that link the dish assembly to the HPAs and electronics enclosures (see Figure 12 and Figure 13). To simplify these interfaces, the high and low voltage cables could be combined into a single cable assembly, and the polarization switch controller could be integrated into the electronics enclosure. Then, all of the cables with the exception of the chiller hoses could be combined into a single cable bundle. This would roughly halve the total number of cable runs.

5.1.1 Waveform Generation Features

In the current version of System-C/X, waveforms are specified by entering parameters into the GUI. More flexibility could be added to this interface by upgrading it to accept pulse descriptor words (PDWs), which is a common method of specifying radar waveforms. The system could also be made to accept raw I/Q files for playback, which would make it a true arbitrary waveform generator. Since the waveform generation is done using SDRs, both of these features can be added to the software without having to make any hardware changes.

5.1.2 HPA Upgrades

The size and weight of the TWTAs used for HPA-C/X could potentially be reduced by switching to SSPAs. By doing so, the liquid chillers could be exchanged

for larger heat sinks and a forced-air cooling system. While the chillers are effective at controlling the TWT temperatures, the chiller adds a significant amount of weight and setup time, and constitutes a single point of failure. With careful SSPA selection, it should be possible to reduce the size and complexity of the system while maintaining the desired peak EIRPs (this might also require tweaking the antenna gains).

5.1.3 Ruggedization

Finally, the System-C/X hardware can be further ruggedized to extend the life of the systems and to reduce the amount of time between repairs. While the systems are reasonably durable, there are several areas where small changes could bring large improvements to the overall system performance. One improvement would be to change plastic bulkhead connectors (e.g., those used for the Ethernet connectors and HPA high voltage cables) to more robust military-specification components. Another simple improvement would be to use higher quality transport cases for the electronics enclosure and HPA submodules.

REFERENCES

Balanis, C. A. (2015). *Antenna theory: analysis and design*. John wiley & sons.

Bliss, D. W. (2021). *Modern Communications: A Systematic Introduction*. Cambridge University Press.

Center, N. A. W. (1997). Electronic warfare and radar systems engineering handbook. *Electronic Warfare Division, Pont Mugu, CA*.

Friis, H. T. (1946). A note on a simple transmission formula. *Proceedings of the IRE*, 34(5):254–256.

Gordon, S. (2019). *Highly Multiplexed Superconducting Detectors and Readout Electronics for Balloon-Borne and Ground-Based Far-Infrared Imaging and Polarimetry*. Arizona State University.

Huang, Y. (2021). *Antennas: from theory to practice*. John Wiley & Sons.

Hunter, I. (2001). *Theory and design of microwave filters*. Number 48. Iet.

Lyons, R. G. (1997). *Understanding digital signal processing, 3/E*. Pearson Education India.

Montgomery, R. and Courtney, P. (2017). Solid-state pas battle twtas for ecm systems. *Microwave Journal, Jun*.

Pierce, J. and Field, L. M. (1947). Traveling-wave tubes. *Proceedings of the IRE*, 35(2):108–111.

Pozar, D. M. (2011). *Microwave engineering*. John wiley & sons.

Sklar, B. (2001). *Digital communications*, volume 2. Prentice hall Upper Saddle River, NJ, USA:.

Skolnik, M. I. (1980). Introduction to radar systems. *New York*.

Smith, S. W. et al. (1997). The scientist and engineer's guide to digital signal processing.

Stimson, G. W. (2014). Introduction to airborne radar, ed.

Wyglinski, A. M., Getz, R., Collins, T., and Pu, D. (2018). *Software-defined radio for engineers*. Artech House.